Biogenic hydroxysulfate green rust, a potential electron acceptor for SRB activity

Asfaw Zegeye, Lucie Huguet, Mustapha Abdelmoula, Cédric Carteret, M. Mullet, Frédéric Jorand

Biogenic hydroxysulfate green rust, a potential electron acceptor for SRB activity

Running title: Microbial reduction of GR(SO_4^{2-}).

Asfaw Zegeye, Lucie Huguet, Mustapha Abdelmoula,* Cédric Carteret, Martine Mullet, and Frédéric Jorand

[1]Laboratoire de Chimie Physique et Microbiologie pour l'Environnement (LCPME), UMR 7564 CNRS-Université Henri Poincaré-Nancy 1, 405, rue de Vandœuvre, F-54600 Villers-lès-Nancy, France.

Corresponding author

E-mail: abdelmoula@lcpme.cnrs-nancy.fr

Revised version

Submitted : 06/25/07

ABSTRACT

Microbiological reduction of a biogenic sulfated green rust (GR2(SO_4^{2-})), was examined using a sulfate reducing bacterium (*Desulfovibrio alaskensis*). Experiments investigated whether GR2(SO_4^{2-}) could serve as a sulfate source for *D. alaskensis* anaerobic respiration by analyzing mineral transformation. Batch experiments were conducted using lactate as the electron donor and biogenic GR2(SO_4^{2-}) as the electron acceptor, at circumneutral pH in unbuffered medium. GR2(SO_4^{2-}) transformation was monitored with time by X-ray diffraction (XRD), Transmission Mössbauer Spectroscopy (TMS), Diffuse Reflectance Infrared Fourier Transform Spectroscopy (DRIFTS), Transmission Electron Microscopy (TEM) and X-ray Photoelectron Spectroscopy (XPS). The reduction of sulfate anions and the formation of iron sulfur mineral were clearly identified by XPS analyses. TMS showed the formation of additional mineral as green rust (GR) and vivianite. XRD analyses discriminated the type of the newly formed GR as GR1. The formed GR1 was GR1(CO_3^{2-}) as indicated by DRIFTS analysis. Thus, the results presented in this study indicate that *D. alaskensis* cells were able to use GR2(SO_4^{2-}) as an electron acceptor. GR1(CO_3^{2-}), vivianite and an iron sulfur compound were formed as a result of GR2(SO_4^{2-}) reduction by *D. alaskensis*. Hence, in environments where geochemical conditions promote biogenic GR2(SO_4^{2-}) formation, this mineral could stimulate the anaerobic respiration of sulfate reducing bacteria.

1. INTRODUCTION

Green rusts (GRs) are Fe(II-III) layered double hydroxysalts hydroxides belonging to the sjögrenite-pyroraurite mineral class (Génin et al., 1998; Hansen, 1989). The crystallographic structure consists of positively charged trioctahedral metal sheets alternating with negatively charged hydrated interlayers of anions. X-ray diffraction analysis distinguishes two different types of GR, namely GR1 and GR2 (Bernal et al., 1959). GR1 contains planar or spherical anions (e.g., CO_3^{2-}, Cl^-) (Abdelmoula et al., 1996; Refait et al., 1998), whereas GR2 contains non-planar anions (*e.g.,* SeO_4^{2-}, SO_4^{2-}) (Hansen et al., 1994; Refait et al., 2000; Simon et al., 2003). Direct evidence for the presence of green rusts in hydromorphic soils (Abdelmoula et al., 1998; Feder et al., 2005; Trolard et al., 1997) and their occurrence during corrosion of iron in drinking water pipes (Stampfl, 1969) or in seawater (Génin et al., 1993; Olowe et al., 1989; Refait et al., 2003a) have been widely reported.

Fe(II-III) minerals such as green rust and magnetite, that could be formed through bacterial Fe(III) reduction (Fredrickson et al., 1998; Glasauer et al., 2003; Ona-Nguema et al., 2002; Zachara et al., 2002), are commonly generated as a result of interaction between microrganisms and their surrounding environment (Konhauser, 1997). These biogenic Fe(II-III) minerals are relevant because they could support bioreduction processes by serving as electron acceptors. Therefore, an understanding of the chemical and biological factors controlling the reduction of these minerals appears to be essential for predicting the impact of microbial anaerobic respiration (Fredrickson et al., 1998). For instance, *S. putrefaciens* strain CN32 and MR-1 can use Fe(III) in crystalline biogenic magnetite as electron acceptors (Dong et al., 2000). To the best of the author's knowledge, the availability of other Fe(II-III) minerals, such as green rust (GRs), to assist the respiration of anaerobic bacteria has not yet been investigated.

The GR2(SO_4^{2-}) and sulfate reducing bacteria (SRB) are found to be associated with corrosion products in seawater (Olowe et al., 1990). SRB are the most extensively studied microorganisms in relation to biocorrosion and are considered as the main causative organisms in microbiologically influenced corrosion (MIC) in seawater (Beech and Gaylarde, 1999; Geesey et al., 2000; Hamilton and Lee, 1995). These bacteria use organic sources or H_2 as electron donors and sulfate as the final electron acceptor during their anaerobic respiration (Hamilton, 1998; Marchal, 1999). Lee et al., (2005) showed the co-existence of SRB and dissimilatory iron reducing bacteria (DIRB) on carbon steel submerged in ocean water. The formation of GR2(SO_4^{2-}) has been shown to occur during bio-reduction of lepidocrocite in *S. putrefaciens* culture (Ona-Nguema et al., 2004; Zegeye et al., 2005). Therefore, the sulfate in the mineral could serve as an electron acceptor for SRB anaerobic respiration. Thus, DIRB could supply the electron acceptor for SRB from the product of their own anaerobic Fe(III) respiration allowing the SRB activities.

In a previous study Zegeye et al., (2005), have focused on the formation and the characterization of a biogenic GR2(SO_4^{2-}). The present study was initiated to examine the potential for biotically formed GR2(SO_4^{2-}) to serve as a sulfate source for the anaerobic respiration of SRB. Because the initial green rust mineral was formed by a dissimilatory iron reducing bacterium, we examine what can be considered as a biotically coupled process.

The solid phase was inoculated with strictly anaerobic sulfate reducing bacteria (*Desulfovibrio alaskensis*), recovered from a soured oil well, using lactate as the electron donor in unbuffered medium. We specifically focus on the characterization of mineral phase transitions during the microbial reduction of sulfate from the biotic GR2(SO_4^{2-}). We used X-ray Diffraction (XRD), Transmission Mössbauer Spectroscopy (TMS), Diffuse Reflectance Infrared Fourier Transform Spectroscopy (DRIFTS), Transmission Electron Microscopy

(TEM) and X-ray Photoelectron spectroscopy (XPS) to investigate the solid phase transformation resulting from *D. alaskensis* activity.

2. MATERIALS AND METHODS

2.1. GR2(SO_4^{2-}) mineral

The GR2(SO_4^{2-}) was obtained by bacterial dissimilatory Fe reduction as described in Zegeye et al., (2005). Briefly, the GR resulted from the reduction of lepidocrocite (γ-FeOOH) by *Shewanella putrefaciens* CIP 8040 using H_2 as electron donor. According to XRD, DRIFTS and TMS analyses, about 55 % of γ-FeOOH was transformed into a single iron(II-III)-bearing mineral *i.e* GR2(SO_4^{2-}).

After 3 months of incubation, the mixture of 45 % γ-FeOOH and 55 % GR2(SO_4^{2-}) was recovered by centrifugation and subsequently washed three times with sterilized and oxygen-free 18 MΩ cm^{-1} resistivity nano-pure water. This procedure ensures the removal of adsorbed sulfate from the GR2(SO_4^{2-}) (Zegeye et al., 2005). One should note that the mineral mixture was not autoclaved, to avoid any transformation of GR2(SO_4^{2-}) by heating. However, a layer consisting of *S. putrefaciens* cells that was formed on top of the biogenic mixture pellet was carefully removed with a sterile spatula after each washing step and no *S. putrefaciens* cell in the pellet was detected by plate counts method on trypticase soy agar (TSA). The minerals were then dried for 24 hours in an anaerobic chamber (N_2:H_2, 95:5) under a 90 % relative humidity. XRD analysis indicated that the GR2(SO_4^{2-}) was not transformed during the washing and drying processes (data not shown). The GR2(SO_4^{2-}) in the dried mixture was used as the sole sulfate reservoir and electron acceptor for *D. alaskensis*.

2.2. Bacteria and media

The *Desulfovibrio alaskensis* strain, initially isolated from a soured oil reservoir in Prudhoe Bay, Alaska, was provided by Pr. Iwona Beech (Portsmouth University). The cells were cultivated to stationary growth phase at 30 °C in trypticase soy broth (TSB) supplemented with 5 $g.L^{-1}$ $MgSO_4$ in an anaerobic (N_2:H_2, 95:5) chamber (Coy laboratory product). Cells were harvested by centrifugation, washed twice and concentrated in 35 mL of a sterile O_2 free NaCl 0.7% solution. This bacterial suspension was used to inoculate batches containing the mixture of lepidocrocite and GR2(SO_4^{2-}).

2.3. Bioreduction assays

The batch medium (sodium lactate, 3.5 g L^{-1}; $MgCl_2$•$6H_2O$, 3.4 g L^{-1}; NaCl, 0.3 g L^{-1}; K_2HPO_4, 0.5 g L^{-1}; $CaCl_2$, 0.1 g L^{-1}) was sterilized by autoclaving and purged with filter sterilized N_2. 80 mL of the medium was dispensed into sterile 100 mL flasks and crimp sealed with butyl rubber stoppers. Samples of 0.402 ± 0.002 g of biologically produced GR2(SO_4^{2-}) (containing γ-FeOOH) were introduced into the flasks in the anaerobic chamber. *D. alaskensis* cell suspensions were added to produce a final concentration of 4.4×10^8 colony forming unit (CFU) CFU mL^{-1}. A pH of 7.5 was measured after all components were mixed. Cultures were incubated at 30 °C in darkness and each treatment was replicated four times. A first control sample was prepared with 0.07 g of lepidocrocite with *D. alaskensis* cells, in order to control if *D. alaskensis* was able to reduce Fe(III) without sulfate under the experimental conditions. A second control sample was cell free and otherwise identical to the biotic samples. These controls were checked for mineral stability, after 25 days of incubation in the reduction

media, by XRD analysis (data not shown). A third control was carried out with an abiotically formed GR2(SO_4^{2-}) otherwise identical to the biotic sample in order to determine if the presence of γ-FeOOH affect the mineralogical bio-transformation of the GR2(SO_4^{2-}). This control served also to check if a residual activity of *S. putrefaciens* cells in the biotic assays could modify the transformation of GR2(SO_4^{2-}) by *D. alaskensis*. This control was analyzed for mineral transformation after 3 and 20 days of incubation by XRD and DRIFTS.

2.4. Chemical Analysis

At selected time points, 1 mL of suspension was removed from the reduction medium, in the anaerobic chamber, introduced directly into 1 mL HCl (2N) and incubated for one week. This 1N HCl extraction ensures the dissolution of the biogenic Fe(II). Fe^{2+} concentration was then determined by the modified 1,10-phenanthroline method (Fadrus and Maly, 1975).

2.5. Instrumentation

2.5.1. X-ray diffraction

After sampling, the suspension was filtered through 0.45 µm pore membrane filters under N_2:H_2 (95:5) atmosphere. The obtained wet paste was spread out on a glass plate and coated with glycerol to inhibit oxidation (Hansen, 1989). The XRD data were collected with a D8 Bruker diffractometer, equipped with a monochromator and a position-sensitive detector. The X-ray source was a Co anode (λ = 0.17902 nm). The diffractogram was recorded in the 3 – 64 2θ range, with a 0.0359° step size and a collecting time of 3 seconds per point.

2.5.2. Transmission Electron Microscopy

Transmission electron microscopy was conducted using a CM20/STEM Philips with a voltage of 200 kV. One drop of the suspension was laid on an amorphous carbon-coated grid and loaded into the analysis holder of the microscope under 10^{-8} Torr vacuum.

2.5.3. Transmission Mössbauer Spectroscopy

Mössbauer spectra were obtained from a constant acceleration Mössbauer spectrometer connected to a 512 multichannel analyzer. The amplifier output and the drive mechanism were manufactured by Halder Electronics GmbH. The detector consisted of an NaI(Tl) scintillation counter. The source of 50 mCi ^{57}Co in Rh matrix was maintained at room temperature. The spectrometer was calibrated with a 25-μm foil of alpha-Fe at room temperature and isomer shifts were given relative to this reference. Aliquots were taken from the well-homogenized medium and the iron bearing particles were concentrated by filtration (0.45 μm pore size) under (N_2:H_2, 95:5) atmosphere inside an anaerobic chamber. The sample absorbers were immediately cooled to the liquid nitrogen temperature and maintained until measurements were taken. To prevent oxidation, they were quickly transferred to the cryostat under an inert He atmosphere before measurements. The maximum area density of Fe in the samples was approximately 10 mg cm^{-2} and thickness effects were assumed to be negligible. The spectra were fitted with the Recoil Software of Lagarec and Rancourt (http://www.physics.uottawa.ca/~recoil) (Lagarec and Rancourt, 1997), using the Lorentzian or pseudo-Voigt method. The parameters resulting from any computer fitting must be

mathematically and physically significant (chi^2 minimization); in particular the width of all lines must be small enough.

2.5.4. Diffuse Reflectance Infrared Fourier Transform Spectroscopy

A Fourier transform infrared spectrometer (Perkin-Elmer 2000), equipped with a KBr beam splitter and a DTGS detector, was used for sample characterization by vibrational spectroscopy. The spectral resolution and the total acquisition time were 4 cm^{-1} and 10 min, respectively. FTIR spectra in diffuse reflectance mode were collected using Harrick DRA-2CI equipment. To perform the analysis, the washed and dried samples were first diluted in a KBr matrix (5 wt.%). The samples were then mixed gently with KBr in an agate mortar, so that the mixtures were not subjected to elevated pressures. The samples were prepared in an anaerobic chamber (N_2:H_2, 95:5) to avoid exposure to oxygen and enclosed in an airtight Harrick HVC-DRP cell with KRS-5 windows for infrared analysis. The reflectances R_s of the sample and R_r of pure KBr, used as a non-absorbing reference powder, were measured under the same conditions. Iron oxide-hydroxide reflectance is defined as $R = R_s/R_r$. The spectra are shown in pseudo-absorbance (-logR) mode.

2.5.5. X-Ray Photoelectron Spectroscopy

X-ray photoelectron spectra were recorded with a KRATOS Axis Ultra instrument using monochromatic Al Kα X-rays (hν =1486.6 eV) operated at 150 W. The samples were pressed onto a Cu tape on a holder and introduced into the spectrometer. The base pressure of the analytical chamber was approximately 10^{-9} Torr. The spectra were collected at normal (90°) take-off angle. Survey scans were used to determine the chemical elements at the sample

surface. They were acquired with a pass energy of 160 eV and a X-ray spot size of 0.3 × 0.7 mm. Narrow region electron spectra were used to determine the chemical state information. They were acquired with an analyser pass energy of 20 eV and an X-ray spot size of 0.3 x 0.7 mm. The spectral resolution is 0.5 eV. The binding energy was calibrated by assigning the C(1s) peak to 284.6 eV. Spectra for sulfur were fitted using a Shirley Background (Shirley, 1972) and a pseudo-voigt peak model.

3. Results

3.1. Monitoring of biomass, pH and Fe(II)

Concerning the biomass, the cell cultivability has been followed over time. No growth is observed in bioreductions assays, the total cultivable cells remaining stable from 4.4 10^8 CFU.mL^{-1} to 2 10^8 CFU.mL^{-1} during the incubation time. Cultivable cells fall down to 1.0 10^5 CFU.mL^{-1} in the control containing lepidocrocite and SRB without the single potential electron acceptor, the GR2(SO_4^{2-}), indicating that GR is needed to maintain biomass in a steady-state.

Visual changes inside the batch bottles were evident within 3 days. The color of the solid phase changed from blue-green to black, suggesting a mineral transformation. Moreover, the characteristic H_2S odor, escaping from the bottles when aliquots were removed for analyses, signaled the reduction of sulfate anions. Fe(II) concentration in the treatments immediately increases after the inoculation of SRB and during the time of incubation (Fig. 1). The pH remains constant and equal to 7.5 during the experiment. Approximate values of 25 mM were reached, indicating Fe(III) reduction of either γ-FeOOH or GR2(SO_4^{2-}). In the cell free control assay with GR2(SO_4^{2-}), Fe(II) concentrations reached around 8 mM, during the same time of incubation. This suggests a residual activity of *S. putrefaciens* cells since the mixture GR2(SO_4^{2-}) and γ-FeOOH was not sterilized. However, the concentration of Fe(II) in the assay are about 3 times higher than those in the blank experiment, thus indicating an extensive reduction by *D. alaskensis* activity. Higher Fe(II) concentrations than the cell free control were never found in the assay containing only γ-FeOOH with SRB. Thus, the

enhanced reduction of Fe(III) in the presence of the bio-generated GR2(SO_4^{2-}) plus γ-FeOOH is not due to the biotic reduction of γ-FeOOH by *D. alaskensis*.

Taking these different results into consideration, the increase in Fe(II) concentration in the treatments containing SRB cells and the mixture of the bio-generated GR2(SO_4^{2-}) plus γ-FeOOH indicates the abiotic reduction of γ-FeOOH and/or GR2(SO_4^{2-}) by H_2S, which is the reaction product of bacterial sulfate reduction.

3.2. Mineral products of biogenic GR2(SO_4^{2-}) reduction by *D. alaskensis*: evidence of sulfate reduction

3.2.1. X-ray diffraction

Prior to SRB inoculation, the diffraction patterns exhibit only the diffraction lines of the bio-generated GR2(SO_4^{2-}) and γ-FeOOH (Fig. 2A) in agreement with previous data (Hansen et al., 1994; Ona-Nguema et al., 2004; Simon et al., 1997; Zegeye et al., 2005). Experimental GR2 *d*-spacings are similar to those previously obtained in biotic and abiotic conditions for GR2(SO_4^{2-}). After 3 days of incubation with *D. alaskensis*, the XRD pattern exhibits diffraction lines of GR2(SO_4^{2-}) and γ-FeOOH, the intensity of which are both strongly decreased. An additional reflection line with *d*-spacing characteristic of vivianite [$(Fe_3(PO_4)_2 \bullet 8H_2O$] (0.684 nm, 14.9° 2$\theta$) is also observed. Significant mineralogical changes are revealed by the XRD pattern after 20 days of incubation. X-ray diffraction peaks of GR2 and γ-FeOOH disappear and new lines ascribable to the GR1 are observed, which was the predominant product after 20 days of incubation. This GR1 is a GR1(CO_3^{2-}) as established by DRIFTS analysis (Drissi et al., 1995; Ona-Nguema et al., 2002). The peak at 0.684 nm (14.9° 2θ) assigned to vivianite is also present. The X-ray diffraction patterns of assay containing the

biotic GR2(SO_4^{2-}) plus γ-FeOOH do not show further changes after 300 days of incubation and are consistent with the presence of a mixture of GR1(CO_3^{2-}) and vivianite.

The same mineralogical transformation is observed in the control run with the chemically synthesized GR2(SO_4^{2-}) (Fig. 2B). Indeed, characteristic peaks of vivianite and GR1 are revealed after 3 and 25 days of incubation respectively. This control indicates that the presence of γ-FeOOH does not affect the biotransformation of the biogenic GR2(SO_4^{2-}). It also shows that biotransformation of the GR2(SO_4^{2-}) was not due to a residual activity of *S. putrefaciens* cells but to *D. alaskensis* cells. The cell-free control does not show any GR2(SO_4^{2-}) transformation. This observation further supports the idea that the observed mineral transformation is attributable to the activity of *D. alaskensis* cells.

3.2.2. Mössbauer Spectroscopy

Mössbauer measurements (between 215 and 13 K) were performed to follow the mineralogical transformation during the incubation period (Fig. 3). In contrast to XRD, this method provides information on compounds that do not exhibit long-range structural order (poorly crystalline solids). The starting mineral exhibits doublets D_1 and D_2 corresponding to GR and the doublet D_L is assigned to paramagnetic Fe^{3+} in lepidocrocite at 77 K. The doublet D_1 corresponds to the ferrous state, whereas the D_2 is assigned to the ferric state. These characteristic features indicate that these components are associated with ordered arrangements of Fe^{2+} and Fe^{3+} in the brucite sheet. As expected, the Fe(II)/Fe(III) ratio in the GR formed is about 2. It was not possible to discriminate between GR1 and GR2 by TMS because this technique is sensitive to the local environment of the probe nucleus, Fe. The hyperfine parameters result from the perturbation of these nuclear levels by their electronic environment. In contrast, XRD is a global method (crystallographic) technique and allow to

observe the structural specificity of the GRs which can intercalate three dimensional anions (GR2) or planar anions (GR1).

In agreement with XRD the Mössbauer spectrum obtained after 3 days of incubation, displays two new ferrous components assigned to vivianite. These paramagnetic quadrupole doublets correspond to vivianite with two crystal sites for Fe(II). D_1 is assigned to vivianite-Fe1 and D_2 to vivianite-Fe2. The TMS analysis shows also a new magnetic component which exhibited sextets, S_A and S_B. The hyperfine parameters of this spectrum are S_A (δ = 0.47 mm s^{-1}; H = 475 kOe) and S_B (δ = 0.84 mm s^{-1}; H = 277 kOe). This phase is not identified by XRD analysis, probably due to its poor crystallinity and/or its low amont. In spite of the appearance of a new Fe(II) component ascribable to vivianite, the total amount of Fe(II) is smaller than that of Fe(III), which corresponds to two overlapping doublets (Fe(III) of lepidocrocite and GR respectively). The 215 K Mössbauer spectral pattern for the bio-reduced material after 20 days of incubation is similar to the pattern for 3 days of incubation, except that the total amount of paramagnetic Fe(III) decreases substantially. The decrease of the lepidocrocite doublets is probably due to its reductive dissolution by H_2S that was produced by sulfate reduction. After 300 days of incubation, the paramagnetic components attributable to vivianite and the GR are always present; in addition, the intensity of the magnetically ordered component increased. This component is probably iron sulfide in the form of greigite (Fe_3S_4) supported by the values of the hyperfine magnetic fields *H* of its two sextets (280 and 355 kOe). Greigite, Fe_3S_4, is the sulfur analogue of magnetite (Fe_3O_4) and has a similar inverse spinel structure.

3.2.3. Characterization of anions in the solid phase

Figure 4A illustrates the DRIFTS spectral changes occurring after 300 days of incubation of *D. alaskensis*. Spectrum (a) exhibits the typical features of sulfate green rust (Ona-Nguema et al., 2004; Peulon et al., 2003; Zegeye et al., 2005): bands arising from the brucite-like sheets at 515, 780, 880 and 1550 cm^{-1} and bands due to the intercalated sulfate at around 620/660 and 1105/1138 cm^{-1}. In addition to these GR spectra lines, this spectrum reveals the presence of γ-FeOOH, with a characteristic absorption at 1022 cm^{-1} (Zegeye et al., 2005). After 300 days of incubation (spectrum b), it is noteworthy that the bands associated with brucite-like sheets are almost unaffected. In contrast, both the characteristic signals of sulfate and the sharp band due to lepidocrocite have disappeared. A large and intense band at 1000 cm^{-1}, with shoulders at 1047, 1101 and 1142 cm^{-1}, assigned to a phosphate solid (Farmer, 1974) appears concomitantly with a very intense peak at 1351 cm^{-1} with a shoulder at 1395 cm^{-1} assigned to the carbonate ions intercalated in a GR1 structure (Peulon et al., 2003; Ona-Nguema et al., 2004).

The same result is observed for the control run with the abiotic GR2(SO_4^{2-}) (Fig. 4B). The spectrum (a) exhibits the typical features of a sulfate GR as described above. The characteristic signals of sulfate have disappeared after 20 days of incubation (spectrum b). This results indicate that γ-FeOOH doesn't interfere with sulfate reduction in the assay containing the biogenic GR2(SO_4^{2-}). This result corroborates the conclusions obtained by XRD, which indicate that the transformation of GR2(SO_4^{2-}) was due to the activity of *D. alaskensis*.

3.2.4. Surface Analysis by XPS

Figures 5 and 6 show the high resolution S(2p) and Fe($2p_{3/2}$) spectra for the mixture GR2(SO_4^{2-})/γ-FeOOH and the products obtained after 300 days of incubation (GR1(CO_3^{2-}

)/vivianite) respectively. S($2p_{3/2}$) and Fe($2p_{3/2}$) binding energies for various model compounds are listed in Table 1.

The S(2p) spectra are fitted using doublets $2p_{1/2}$ and $2p_{3/2}$ separated by a spin-orbit splitting of 1.2 eV (Fig. 5). The S($2p_{1/2}$) peak area is constrained to one-half of the area of S($2p_{3/2}$) peak. As expected, a good fit of the spectrum of the GR2(SO_4^{2-})/γ-FeOOH initial mixture is obtained using a doublet with $2p_{3/2}$ binding energy at 168.2 eV corresponding to sulfate species (Table 2, Fig. 5). No other sulfur species are observed. To adequately fit the S(2p) spectrum of the final products, three doublets are required (Table 2). The $2p_{3/2}$ binding energy of the major doublet at 160.9 eV is typically attributed to monosulfide species. Monosulfide species represent 66% of the whole signal. Additionally, two others doublets are fitted to take into account for the high energy tail of the spectrum. The $2p_{3/2}$ components are located at 161.8 and 163.3 eV and may correspond to disulfide (S_2^{2-}) and polysulfides (S_n^{2-}) respectively. The presence of disulfide and polysulfide species was previously reported by Herbert et al. (1998) at the surface of iron monosulfide precipitated in the presence of SRB.

The broad Fe($2p_{3/2}$) spectra present a major contribution occurring near 710.5 eV and 710.7 eV for the initial mixture and the final products respectively (Fig. 6). To the best of the authors knowledge, the assignment of Fe(II) and Fe(III) features in XPS spectra of green rusts is not reliably established yet. The reasons for this have to do with the small binding energy difference between the Fe($2p_{3/2}$) peaks of Fe(II) and Fe(III) coordinated by oxygen, the variety of chemical environments for Fe in GR, and the multiplet structure of Fe XPS spectra. This is probably explained by the small difference in binding energy range between combined to the multiplet structure of iron. Our spectra are made more complex by the presence of several Fe-containing phases. No attempt was therefore made to fit the Fe($2p_{3/2}$) spectra. However, the main features observed in Figure 6 are not surprisingly the sum of Fe(II) and Fe(III) contributions, both corresponding to iron-oxygen bond types in (oxyhydr)oxides

(Table 1). Note that the Fe(II)-O component located at 710 eV is clearly evidenced in the spectrum relative to the initial mixture of GR2(SO_4^{2-})/γ-FeOOH. Of interest is the shoulder that only appears at the low energy side of the Fe($2p_{3/2}$) spectrum of the final products. The corresponding binding energy is around 707 eV, which typically falls in the range reported for Fe(II)-S compounds (Table 1). Note that the binding energy range of Fe(II) bound to S is much slower than that of Fe(II)-O, so that the discrimination between these two components is unambiguous.

XPS data are clearly consistent with the microbial reduction of sulfate. Iron (oxyhydr) oxides are dominantly observed and the formation of an Fe(II)-S compound is suggested.

3.2.5. Transmission electron microscopy

TEM images of the inoculated and un-inoculated treatments incubated for 20 days illustrate the presence of numerous crystals. In the control treatment, large hexagonal crystals assigned to GR2(SO_4^{2-}) and some vivianite crystals are also observed (data not shown). In the inoculated treatments, two additional mineral phases appear, GR1(CO_3^{2-}) and a highly aggregated mineral structure (Fig. 7A). The elemental analysis of this structure yields prominent S and Fe peaks on EDX spectrum with a S/Fe ratio of about 1 (Fig. 7B), thus indicating the probable formation of an Fe-S compound. The SAED pattern of this mineral exhibits a ring-like powder pattern (not shown) consistent with a poor degree of crystallinity. Thus, unequivocal assignment to a particular Fe-S mineral is not possible.

4. Discussion

The experimental results define two major findings. The first one demonstrates that sulfate anions from a biogenic GR2(SO_4^{2-}) serve as sulfate pool for *D. alaskensis* respiration. The second one reveals that GR1(CO_3^{2-}) and iron sulphur minerals are formed as biogenic products of SRB activity. The formation of vivianite is also observed due to the presence of phosphate in the culture medium.

4.1. Bio-reduction of GR2(SO_4^{2-})

Under the experimental conditions, the SO_4^{2-} from the GR2(SO_4^{2-}) was accessible for *D. alaskensis* anaerobic respiration with lactate as the electron source. Indeed, the DRIFTS analysis revealed the disappearance of sulfate bands after 300 days of incubation, suggesting the reduction of sulfate anions by SRB. The XPS analysis corroborates this result as no sulfate signal was observed after the incubation period. The simplified chemical reaction is:

$$2CH_3CHOHCOO^- + SO_4^{2-} = 2CH_3COO^- + 2HCO_3^- + H_2S \quad \{1\}$$

The mechanisms by which SRB acquire the sulfate anions trapped in the GR2(SO_4^{2-}) structure has not been yet established. Laboratory studies have demonstrated that some SRB can reduce sulfate anions bound in minerals by an energy-conserving process (Katrnachuk et al., 2002; Kowalski et al., 2003). These studies highlight the dissolution of the solid phase prior to sulfate reduction. Moreover, the dissolution process could be accelerated by the production of extra-cellular polymeric substances by SRB (Beech and Cheung, 1995; Zinkevich et al., 1996). These findings suggest that dissolution of the mineral occurred prior to sulfate reduction which is in agreement with the biochemical pathway of sulfate reduction

by SRB. It is preceded by sulfate ion transport into the cells and followed by sulfate activation through ATP sulfurylase (Hamilton, 1998). Thus, it seems likely that the dissolution of GR2(SO_4^{2-}) occurred prior to sulfate anions uptake for *D. alaskensis* anaerobic respiration. The mechanistic pathway of how SRB utilize the sulfate from the GR2(SO_4^{2-}) (*in situ* or *ex situ* reduction) would require a dedicated and through investigation and is beyond the scope of this work.

Hydrogen sulfide is a product of anaerobic sulfate reduction. The reaction of dissolved H_2S with iron oxides has been well documented and was proposed to occur *via* a reductive dissolution mechanism with strong pH dependence (Peiffer et al., 1992; Poulton, 2003; Poulton et al., 2002; Yao and Millero, 1996). In the present study carried out at a pH value of around 7, total Fe(II) (solid and soluble phase) concentration increased when the mixture of GR2(SO_4^{2-}) and γ-FeOOH was incubated with SRB. As Fe(II) was not detected in the treatment containing only γ-FeOOH, it seems that the Fe(III) reduction observed in these assays was due to an inorganic reduction of Fe(III) by H_2S rather than enzymatic activity of bacterial cells. This hypothesis is corroborated by an earlier study that suggests an enhancement of the alteration of a Fe-rich clay mineral via biogenic sulfide during sulfate reduction (Yi-Lang et al., 2004). Because H_2S is reactive towards Fe(III), hydrogen sulfide may also influence the dissolution of GR2(SO_4^{2-}).

4.2. The by-product of GR2(SO_4^{2-}) bioreduction

TMS and XRD analyses showed the formation of vivianite in the reduction media. In agreement with previous studies vivianite is formed rapidly at circumneutral pH (Fredrickson et al., 1998; Kukkadapu et al., 2004). The rate of vivianite formation was greater than that of GR1(CO_3^{2-}) under our experimental conditions. Indeed after 3 days of incubation,

vivianite is the only alteration product in the XRD spectra. This trend was also observed during the bioreduction of ferrihydrite in a phosphate containing media by *S. putrefaciens* CN32 (Kukkadapu et al., 2004). The formation of vivianite in abiotic or biotic systems requires the reaction between ferrous ions and dissolved phosphate anions. The increase in Fe(II) concentration during the incubation of the mixture of GR2(SO_4^{2-}) plus γ-FeOOH with SRB supply Fe(II) ions for the precipitation of vivianite. However, the characteristic vivianite line (0.684 nm, 14.9° 2θ) was also observed after 25 days of incubation in the control experiments (data not shown). The formation of this mineral could be explained by the reaction between aqueous Fe^{2+} ions which were in equilibrium with the GR2(SO_4^{2-}) (Bourrié et al., 1999) and the dissolved phosphate anions present in the medium. The precipitation of vivianite in solution containing high level of phosphate and in presence of GR2(SO_4^{2-}) was also observed in abiotic assay (Hansen and Inge, 1999). Therefore, it was not possible to determine the contribution of bacterial activity to vivianite formation. The Fe(II) in vivianite probably originates from both GR2(SO_4^{2-}) and γ-FeOOH.

Lactate oxidation coupled with sulfate reduction resulted in an increase in carbonate anions (as bicarbonate) within the culture media. DRIFTS and XRD analyses conclusively showed the formation of GR1(CO_3^{2-}) in our experiments. TMS hyperfine parameters indicated that the Fe(II)/Fe(III) ratio of the biogenic GR1(CO_3^{2-}) was around 2 (Drissi et al., 1995, Ona-Nguema et al., 2002). No GR(PO_4^{3-}) formed in contrast to the study of Parmar et al., (2001) who attribute the precipitation of GR(PO_4^{3-}) to phosphate in the reduction media. In contrast, Benali et al., (2001) did not observe the formation of GR(PO_4^{3-}) during the incubation of a GR1(CO_3^{2-}) in a phosphate rich media (0.06 M, Na_2HPO_4). Accordingly, Kukkadapu et al., (2004) suggested a higher affinity for carbonate rather than for phosphate during GR formation. Moreover Bocher et al., (2004) demonstrated that phosphate anions

adsorbed preferentially upon the lateral faces of the GR1(CO_3^{2-}) but do not penetrate in the brucite sheet, thus stabilizing the Fe(II-III) mineral.

The formation of FeS compounds such as greigite (Fe_3S_4), mackinawite (FeS_{1-x}, $0 < x < 0.07$) or pyrite (FeS_2) in field settings was often attributed to the presence of sulfate-reducing bacteria (Herbert et al., 1998; Neal et al., 2001; Popa and Kinkle, 2000). In agreement with TEM and TMS analyses, XPS analysis also evidenced the formation of a Fe-S compound. The binding energy of the main S(2p) component (Figure 6) is in agreement with that reported for poorly crystallized compounds such as mackinawite FeS_{1-x} $0 \langle x \langle 0.07$ and/or greigite Fe_3S_4. Note that mackinawite is the first iron sulfide phase formed by the precipitation of iron (II) and sulfide S(-II) and that greigite is an oxidation product of mackinawite (Boursiquot et al.,2001). The Fe(2p) spectra of the final products were consistent with the presence of iron sulfide containing phases, but were equivocal with regards to the specific phase present. Herbert et al. (1998) have previously reported the formation of poorly crystallized precipitates of disordered mackinawite and greigite in media containing SRB. Although none of the analytical techniques used in the present study put forward unequivocal evidence as to the nature of iron sulfide mineral formed, the results obtained by TMS analysis suggested the formation of greigite as the best hypothesis. Indeed, Mössbauer spectra displayed a magnetically ordered compound and the fitting indicated that greigite would be the potential candidate.

4.3. Environmental implication

GR2(SO_4^{2-}) is formed during the marine corrosion of iron in aquatic environments (Olowe et al., 1989; Refait et al., 2003b) and SRB are found in close association with the Fe sulfide phase and GR2 corrosion products (Olowe et al., 1990). Moreover a recent study reported that iron and sulfate reducing bacteria colonized a carbon steel submerged in ocean water, indicating the co-existence of DIRB and SRB (Lee et al., 2005).

In an attempt to integrate the data put forward earlier in this study, we propose a scheme of a corrosion process in which DIRB and SRB are implicated (Fig. 8). Our focus is to illustrate a possible interaction between DIRB and SRB with GR2(SO_4^{2-}) playing the central role. In such a consortium, the major interaction illustrated between the two bacterial groups could be described as: the secondary mineral formed by the activity of one group, the DIRB, serves as electron acceptor for the second group, the SRB.

In the microenvironment at a corroded surface, we would expect that SRB cells are not in direct contact with the bulk solution but enclosed in a corrosion tubercle. The formation of GR2(SO_4^{2-}), through DIRB activity (Fig. 8, path 1) or by an abiotic pathway (Fig. 8, path 2), could allow sulfate to become locally concentrated in the biogenic mineral (2 mM cm^{-3}). This mineral could then serve as an electron acceptor reservoir for SRB that can not reach the bulk solution to use sulfate anions for energy production (Fig. 8, path 3). The reduction of aqueous or embedded sulfate coupled to organic matter oxidation would lead to the formation of H_2S and carbonate (Fig. 8, path 4). H_2S subsequently reacts with Fe(III) and/or Fe(II), which form during corrosion, and contributes to the formation of Fe_xS_y compound (Fig. 8, path 5) whereas CO_3^{2-} would react with Fe(II) and Fe(III) to precipitate carbonate green rust (Fig. 8, path 6).

In this study, we demonstrated that sulfate anions of a biogenic GR2(SO_4^{2-}) were available for SRB anaerobic respiration. Since the initial green rust was formed by an iron

reducing bacterium, this study examines what appears to be a biotically coupled process. This lab-based study can contribute to a better understanding of natural systems, which are inherently complex with respect to microorganisms and minerals. In the environment, more than one species would constitute the biofilm on a corroded surface and trophic interactions would not be the only one. Moreover, the environmental chemistry would also be significantly more complex and influence the overall reactions. However, the presence of Fe(II), H_2, $[CHO]_n$ and the different solid phases included in the illustration are widely described in the literature to occur during corrosion processes (Beech and Gaylarde, 1999; De Windt et al., 2003; Dubiel et al., 2002; Geesey et al., 2000; Jeffrey and Melchers, 2003). The schema (Figure 8) is merely a discussion of this study and further investigations are needed to validate the model proposed herein.

ACKNOWLEDGMENTS

The authors acknowledge I. Bihannic from the Laboratoire Environnement et Minéralogie for the XRD analyses and J. Ghanbaja (Nancy I University) for the TEM analyses. We also thank Pr Herbillon Adrien for encouragement and helpful discussion. We are, furthermore, indebted to Dr C. Eggleston and the anonymous reviewers for their helpful comments that improved the text

REFERENCES

Abdelmoula M., Refait P., Drissi S. H., Mihe J. P., and Génin J.-M. R. (1996) Conversion electron Mössbauer spectroscopy and X-ray diffraction studies of the formation of carbonate-containing green rust one by corrosion of metallic iron in $NaHCO_3$ and ($NaHCO_3$ + NaCl) solutions. *Corros Sci* **38**(4), 623-33.

Abdelmoula M., Trolard F., Bourrie G., and Génin J.-M. R. (1998) Evidence for the Fe(II)-Fe(III) green rust "Fougerite" mineral occurrence in a hydromorphic soil and its transformation with depth. *Hyperfine Interactions* **112**(1-4), 235-238.

Arnold R. G., DiChristina T. J., and Hoffmann M. R. (1988) Reductive dissolution of iron(III) oxides by *Pseudomonas* sp. 200. *Biotechnol Bioeng* **32**(9), 1081-1096.

Beech I. B. and Cheung C. W. S. (1995) Interaction of exopolymers produced by sulphate-reducing bacteria with metal ions. *Int Biodeter Biodegr.* **35**, 59-72.

Beech I. B. and Gaylarde C. C. (1999) Recent advances in the study of biocorrosion - an overview. *Rev Microbiol.* **30**, 177-190.

Benali O., Abdelmoula M., Refait P., and Génin J.-M. R. (2001) Effect of orthophosphate on the oxidation products of Fe(II)-Fe(III) hydroxycarbonate: the transformation of green rust to ferrihydrite. *Geochim Cosmochim Acta* **65**(11), 1715-26.

Bernal J. O., Dasgupta D. R., and Mackay A. L. (1959) The oxides and hydroxides of iron and their structural inter-relationships. *Clay Min Bull* **4**, 15-30.

Bocher F., Géhin A., Ruby C., Ghanbaja J., Abdelmoula M., and Génin J.-M. R. (2004) Coprecipitation of Fe(II-III) hydroxycarbonate green rust stabilised by phosphate adsorption. *Solid State Sci* **6**, 117-124.

Bourrié G., Trolard F., Génin J.-M. R., Jaffrezic A., Maitre V., and Abdelmoula M. (1999) Iron control by equilibria between hydroxy-green rusts and solutions in hydromorphic soils. *Geochim Cosmochim Acta* **63**(19-20), 3417-27.

Boursiquot S., Mullet M., Abdelmoula M., Génin J.-M., Ehrahardt J.-J. (2001) The dry oxidation of tetragonal FeS_{1-x}. *Phys Chem Minerals* **28**, 600-611.

De Windt W., Bonn N., Siciliano S. D., and Verstraete W. (2003) Cell density related H_2 consumption in relation to anoxic Fe(0) corrosion and precipitation of corrosion products by *Shewanella putrefaciens*. *Environ Microbiol* **5**, 1192-1202.

Dong H., Fredrickson J. K., Kennedy D. W., Zachara J. M., Kukkadapu R. K., and Onstott T. C. (2000) Mineral transformation associated with the microbial reduction of magnetite. *Chem Geol* **169**, 299-318.

Drissi S. H., Refait P., Abdelmoula M., and Génin J.-M. R. (1995) The preparation and thermodynamic properties of iron(II)-iron(III) hydroxide-carbonate (green rust); Pourbaix diagram of iron in carbonate-containing aqueous media. *Corros Sci* **37**, 2025-41.

Dubiel M., Hsu C. H., Chien C. C., Mansfeld F., and Newman D. K. (2002) Microbial iron respiration can protect steel from corrosion. *Appl Environ Microbiol* **68**(3), 1440-5.

Fadrus H. and Maly J. (1975) Suppression of iron(III) interference in the determination of iron(II) in water by the 1,10-phenanthroline method. *Analyst* **100**, 549-54.

Farmer V. C. (1974) *The infrared spectra of minerals*. Mineralogical society, Monograph 4.

Feder F., Trolard F., Klingelhöfer G., and Bourrié G. (2005) In situ Mössbauer spectroscopy: evidence for green rust (fougerite) in a gleysol and its transformation with time and depth. *Geochim Cosmochim Acta* **69**, 4463-4483.

Fredrickson J. K., Zachara J. M., Kennedy D. W., Dong H., Onstott T. C., Hinman N. W., and Li S.-m. (1998) Biogenic iron mineralization accompanying the dissimilatory reduction of hydrous ferric oxide by a groundwater bacterium. *Geochim Cosmochi. Acta* **62**(19-20), 3239-3257.

Geesey G. G., Beech I. B., Bremer P. J., Webster B. J., and Weel D. B. (2000) Biocorrosion. In *Biofilm II: Process analysis and applications* (ed. J. D. Bryers), pp. 281-325. Wiley-Liss.

Géhin A., Ruby C., Abdelmoula M., Benali O., Ghanbaja J., Refait P., and Génin J.-M. R. (2002) Synthesis of Fe(II-III) hydroxysulphate green rust by coprecipitation. *Solid State Sci* **4**(1), 61-66.

Génin J.-M. R., Olowe A. A., Resiak B., Benbouzid-Rollet N. D., Confente M., and Prieur D. (1993) Identification of sulfated green rust 2 compound produced as a result of microbially induced corrosion of steel sheet piles in a harbour. *Eur Feder Corros* **10**, 162-166.

Génin J. M. R., Abdelmoula M., Refait P., and Simon L. (1998) Comparison of the GR(II) lamellar double hydroxide class with the GR(I) pyroraurite class: Fe(II)-Fe(III) sulphate and selenate hydroxides. *Hyperfine Interact.* **3**, 313-316.

Glasauer S., Weidler P. G., Langley S., and Beveridge T. J. (2003) Controls on Fe reduction and mineral formation by a subsurface bacterium. *Geochim Cosmochim Acta* **67**(7), 1277-1288.

Hamilton W. A. (1998) Bioenergetics of sulphate-reducing bacteria in relation to their environmental impact. *Biodegradation* **9**, 201-212.

Hamilton W. A. and Lee W. (1995) Biocorrosion. In *Sulfate reducing bacteria* (ed. L. B. Larry). Plenum press.

Hansen H. C. B. (1989) Composition, stabilization, and light absorption of iron(II) iron(III) hydroxy-carbonate ('Green rust'). *Clay Miner* **24**(4), 663-9.

Hansen H. C. B., Borggaard O. K., and Sørensen J. (1994) Evaluation of the free energy of formation of Fe(II)-Fe(III) hydroxide-sulphate (green rust) and its reduction of nitrite. *Geochim Cosmochim Acta* **58**, 2599-608.

Hansen H. C. B. and Inge F. P. (1999) Interaction of synthetic sulphate "green rust" with phosphate and the crystallization of vivianite. *Clay Clay Miner* **47**(3), 312-18.

Herbert R. B., Benner S. G., Pratt A. R., and Blowes D. W. (1998) Surface chemistry and morphology of poorly crystalline iron sulfides precipitated in media containing sulfate-reducing bacteria. *Chem Geol* **144**, 87-97.

Jeffrey R. and Melchers R. E. (2003) Bacteriological influence in the development of iron sulphide species in marine immersion environments. *Corros Sci* **45**(4), 693-714.

Katrnachuk O. V., Kurochkina S. Y., and Tuovinen O. H. (2002) Growth of sulfate-reducing bacteria with solid-phase electron acceptor. *Appl Microbiol Biotechnol* **58**, 482-486.

Konhauser K. O. (1997) Bacterial iron biomineralization in nature. *FEMS Microbiol Rev* **20**, 315-326.

Kostka J. and Nealson K. H. (1995) Dissolution and reduction of magnetite by bacteria. *Environ Sci Technol* **29**, 2535-40.

Kowalski W., Holub W., Wolicka D., Przytocka-Jusiak M., and Blaszczyk M. (2003) Sulphur balance in anaerobic cultures of microorganisms in medium with phosphogypsum and sodium lactate. *Archiwum Mineralogiczne*, 33-40.

Kukkadapu R. K., Zachara J. M., Fredrickson J. F., and Kennedy D. W. (2004) Biotransformation of two-line silica-ferrihydrite by a dissimilatory Fe(III)-reducing bacterium: formation of carbonate green rust in the presence of phosphate. *Geochim Cosmochim Acta* **68**, 2799-2814.

Lagarec K. and Rancourt D.G. (1997) Extended Voigt-based analytic lineshape method for determining N-dimensional correlated hyperfine parameters distributions in *Mössbauer spectroscopy.Nucl. Instr.and Meth.in Phys.Res. B* **129**, 266-280.

Lee A. K., Buehler M. G., and Newman D. K. (2006) Influence of dual-spices biofilm on the corrosion of mild steel. *Corros Sci* **48**, 165-178.

Legrand L., Abdelmoula M., Géhin A., Chausse A., and Génin J.-M. R. (2001) Electrochemical formation of a new Fe(II)-Fe(III) hydroxy-carbonate green rust: characterisation and morphology. *Electrochimica Acta* **46**(12), 1815-1822.

Lovley D. R. (2000) Iron(III) and Mn(IV) reduction. In *Environmental microbe-metal interactions* (ed. D. R. Lovley). ASM Press.

Marchal R. (1999) Rôle des bacteries sulfurogènes dans la corrosion du fer. *Oil and Gaz Sci. technol.* **54**, 649-659.

Mcintyre N. S. and Zetaruk D. G. (1977) X ray photoelectron spectroscopic studies of iron oxides. *Anal Chem* **49**, 1521-1529.

Mullet M., Boursiquot S., Abdelmoula M., Génin J.-M., and Ehrhardt J. J. (2002) Surface chemistry and structural properties of mackinawite prepared by reaction of sulfide ions with metallic iron. *Geochim Cosmochim Acta.* **66**, 829-836.

Myers C. R. and Nealson K. H. (1990a) Iron mineralization by bacteria: metabolic coupling of iron reduction to cell metabolism in *Alteromonas putrefaciens* MR-1. In *Iron biominerals* (ed. R. B. a. B. Frankel, R. P.), pp. 131-149. Plenum Press.

Myers C. R. and Nealson K. H. (1990b) Respiration-linked proton translocation coupled to anaerobic reduction of manganese(IV) and iron(III) in *Shewanella putrefaciens* MR-1. *J Bacteriol* **172**(11), 6232-8.

Neal A. L., Techkarjanaruk S., Dohnalkova A., McCready D., Peyton B. M., and Geesey G. G. (2001) Iron sulfide ans dulfur species produced at hematite surfaces in the presence of sulfate-reducing bacteria. *Geochim Cosmochim Acta* **65**, 223-235.

Nealson K. H. and Saffarini D. (1994) Iron and manganese in anaerobic respiration: environmental significance, physiology, and regulation. *Annu Rev Microbiol* **48**, 311-43.

Nesbitt H. W. and Muir I. J. (1994) X-ray photoelectron spectroscopic study of a pristine pyrite surface reacted with water vapor and air. *Geochim Cosmochim Acta* **58**, 4667-4679.

Olowe A. A., Bauer P., Génin J.-M. R., and Guezennec J. (1989) Mössbauer effect evidence of the existence of green rust II transient compounds from bacterial corrosion in marine sediments. *Corros NACE* **45**, 229-35.

Olowe A. A., Génin J.-M. R., and Guezennec J. (1990) Mössbauer effect study of microbially induced corrosion of steel by sulphate reducing bacteria in marine sediments: role of green rust 2. In *Microbially influenced corrosion and deterioration* (ed. N. J. Dowling, M. W. Mitleman, and J. C. Danko), pp. 65-72. University of Tennessee and NACE.

Ona-Nguema G., Abdelmoula M., Jorand F., Benali O., Géhin A., Block J.-C., and Génin J.-M. R. (2002) Iron (II,III) hydroxycarbonate green rust formation and stabilization from lepidocrocite bioreduction. *Environ Sci Technol* **36**(1), 16-20.

Ona-Nguema G., Carteret C., Benali O., Abdelmoula M., Génin J.-M. R., and Jorand F. (2004) Competitive formation of hydroxycarbonate green rust I *vs* hydroxysulphate green rust II in *Shewanella putrefaciens* cultures. *Geomicrobiol J* **21**(3), 79-90.

Parmar N., Gorby Y. A., Beveridge T. J., and Ferris F. G. (2001) Formation of green rust and immobilization of nickel in response to bacterial reduction of hydrous ferric oxide. *Geomicrobiol J* **18**(4), 375-385.

Peiffer S., Dos Santos M., Wehrll B., and Gächter R. (1992) Kinetics and mechanism of the reaction of H_2S with lepidocrocite. *Environ Sci Tech* **26**, 2408-2413.

Peulon S., Legrand L., Antony H., and Chaussé A. (2003) Electrochemical deposition of thin films of green rusts 1 and 2 on inert gold substrate. *Electrochemistry communication* **5**, 208-213.

Popa R. and Kinkle B. K. (2000) Discrimination among iron sulfide species formed in microbial cultures. *J Microbiol Meth.* **42**, 167-174.

Poulton S. W. (2003) Sulfide oxidation and iron dissolution kinetics during the reaction of dissolved sulfide with ferrihydrite. *Chem Geol* **202**, 79-94.

Poulton S. W., Krom M. D., Van Rijn J., and Raiswell R. (2002) The use of hydrous iron (III) oxides for the removal of hydrogen sulphide in aqueous system. *Water Res.* **36**, 825-834.

Pratt A. R., Nesbitt H. W., and Muir I. J. (1994) Generation of acids from mine waste: oxidative leaching of pyrrhotite in dilute H_2SO_4 solutions at pH 3.0. *Geochim Cosmochim Acta*. 58, 5147-5159.

Refait P., Charton A., and Génin J.-M. R. (1998) Identification, composition, thermodynamic and structural properties of a pyroaurite-like iron(II)-iron(III) hydroxy-oxalate Green Rust. *Eur J Sol State Inor* **35**(10-11), 655-66.

Refait P., Gehin A., Abdelmoula M., and Genin J.-M. R. (2003a) Coprecipitation thermodynamics of iron(II-III) hydroxysulphate green rust from Fe(II) and Fe(III) salts. *Corros Sci* **45**(4), 659-676.

Refait P., Memet J.-B., Bon C., Sabot R., and Génin J.-M. R. (2003b) Formation of the Fe(II)-Fe(III) hydroxysulphate green rust during marine corrosion of steel. *Corros Sci* **45**, 833-845.

Refait P., Simon L., and Génin J.-M. R. (2000) Reduction of SeO_4^{2-} anions and anoxic formation of iron(II)-iron(III) hydroxy selenate green rust. *Environ Sci Technol* **34**(5), 819-25.

Roden E. E. and Zachara J. M. (1996) Microbial reduction of crystalline iron (III) oxides: influence of oxide surface area and potential for cell growth. *Environ Sci Technol* **30**, 1618-28.

Schaufuss A. G., Nesbitt H. W., Karito I., Laajalehto K., Bancroft G. M., and Szargan R. (1998) Incipient oxidation of fractured pyrite surfaces in air. *J. Electron Spectros and Related Phenom* **96**, 69-82.

Simon L., Francois M., Refait P., Renaudin G., Lelaurain M., and Génin J.-M. R. (2003) Structure of the Fe(II-III) layered double hydroxysulphate green rust two from Rietveld analysis. *Solid State Sci* **5**, 327-334.

Simon L., Génin J.-M. R., and Refait P. (1997) Standard free enthalpy of formation of Fe(II)-Fe(III) hydroxysulphite green rust one and its oxidation into hydroxysulphate green rust two. *Corros Sci* **39**(9), 1673-85.

Stampfl P. P. (1969) Basic Fe(II)(III)-carbonate in rust. *Corros Sci* **9**, 185-7.

Thomas J. E., Jones C. F., Skinner W. M., and Smart R. C. (1998) The role of surface species in the inhibition of pyrrhotite dissolution in acid conditions. *Geochim Cosmochim Acta* **9**, 1555-1565.

Trolard F., Génin J.-M. R., Abdelmoula M., Bourrié G., Humbert B., and Herbillon A. (1997) Identification of a green rust mineral in a reductomorphic soil by Mössbauer and Raman spectroscopy. *Geochim Cosmochim Acta* **61**, 1107-11.

Yao W. and Millero F. J. (1996) Oxidation of hydrogen sulfide by hydrous Fe(III) oxides seawater. *Marine Chemistry* **52**, 1-16.

Yi-Lang L., Hojatollah V., Sears S. K., Yang J., Deng B., and Zangh C. L. (2004) Iron reduction and alteration of nontronite NAu-2 by sulfate-reducing bacteria. *Geochim Cosmochim Acta* **68**, 3251-3260.

Zachara J. M., Kukkadapu R. K., Fredrickson J. K., Gorby Y. A., and Smith S. C. (2002) Biomineralization of poorly crystalline Fe(III) oxides by dissimilatory metal reducing bacteria (DMRB). *Geomicrobiol J* **19**(2), 179-207.

Zachara J. M., Li S.-M., Kennedy D. W., Smith S. C., and Gassman P. L. (1998) Bacterial reduction of crystalline Fe^{3+} oxides in single phase suspensions and subsurface materials. *Amer Mineral* **83**, 1426-43.

Zegeye A., Ona-Nguema G., Carteret C., Huguet L., Abdelmoula M., and Jorand F. (2005) Formation of hydroxysulphate green rust 2 as a single iron(II-III) mineral in microbial culture. *Geomicrobiol. J.* **22**, 389-399.

Zinkevich V., Bogdarina I., Kang H., Hill M. A. W., Tapper R., and Beech I. B. (1996) Characterization of exopolymers produced by different isolates of marine sulphate-reducing bacteria. *Int Biodete Biodegr* **37**, 163-173.

Table 1

Incubation time and temperature		δ [a] (mm s^{-1})	Δ or 2ε [b] (mm s^{-1})	H^c (kOe)	Relative abundance (%)
t=0	GR	D_1 : 1.27	2.92		36
77 K		D_2 : 0.48	0.44		21
	Lepido	D_L : 0.47	0.62		43
t=3 days	GR	D_1 : 1.24	2.87		16
100 K		D_2 : 0.53	0.39		10
	Lepido	D_L : 0.46	0.73		46
	Vivianite	: 1.33	3.2		7
		: 1.24	2.54		6
	Greigite	: 0.47	-0.14	475	9
		: 0.84	0.02	277	6
t=20 days	GR	D_1 : 1.18	2.6		34
215 K		D_2 : 0.4	0.5		32
	Lepido	D_L: 0.47	0.5		5
	Vivianite	: 1.20	2.96		13
	Greigite	: 0.41	-0.09	419	11
		: 0.85	-0.5	387	4
t=300 days	GR	D_1 : 1.24	2.67		29
13 K		D_2 : 0.45	0.43		17
	Vivianite	: 1.27	3.1		14
	Greigite	: 0.49	0	280	20
		: 0.88	-0.5	355	8
	Iron oxide	: 0.48	-0.15	504	12

(a) Isomer shift relative to metallic iron
(b) Quadrupole splitting or quadrupole shift
(c) Hyperfine magnetic field

Table 2

Species	Binding energy (eV)	References
Fe($2p_{3/2}$)		
Fe(II)-S	706.8	(Mullet et al., 2002)
	707.3	(Herbert et al., 1998)
Fe(II)-O	709.5	(Mcintyre and Zetaruk, 1977)
	709.0	(Thomas et al., 1998)
Fe(III)-S	709.20*	(Pratt et al., 1994)
	709.15*	(Herbert et al., 1998)
Fe(III)-O	710.30*	(Nesbitt and Muir, 1994)
	710.8*	(Schaufuss et al., 1998)
S($2p_{3/2}$)		
S^{2-}	161.3	(Mullet et al., 2002)
	160.9	(Herbert et al., 1998)
S_2^{2-}	162.2	(Herbert et al., 1998)
S_n^{2-}	163.6	(Nesbitt and Muir, 1994)
	163.4	(Thomas et al., 1998)
SO_4^{2-}	168.1	(Thomas et al., 1998)

*Measurements corresponding to the main component of the multiplet peaks

Table 3

BE (eV)	FHWM	Area	Species
	Starting material GR2(SO_4^{2-})		
168.2	1.1	100	sulfate
	T = 300 days		
160.9	0.9	66.0	monosulfide
161.8	1.2	20.1	disulfide
163.3	1.4	13.9	polysulfide

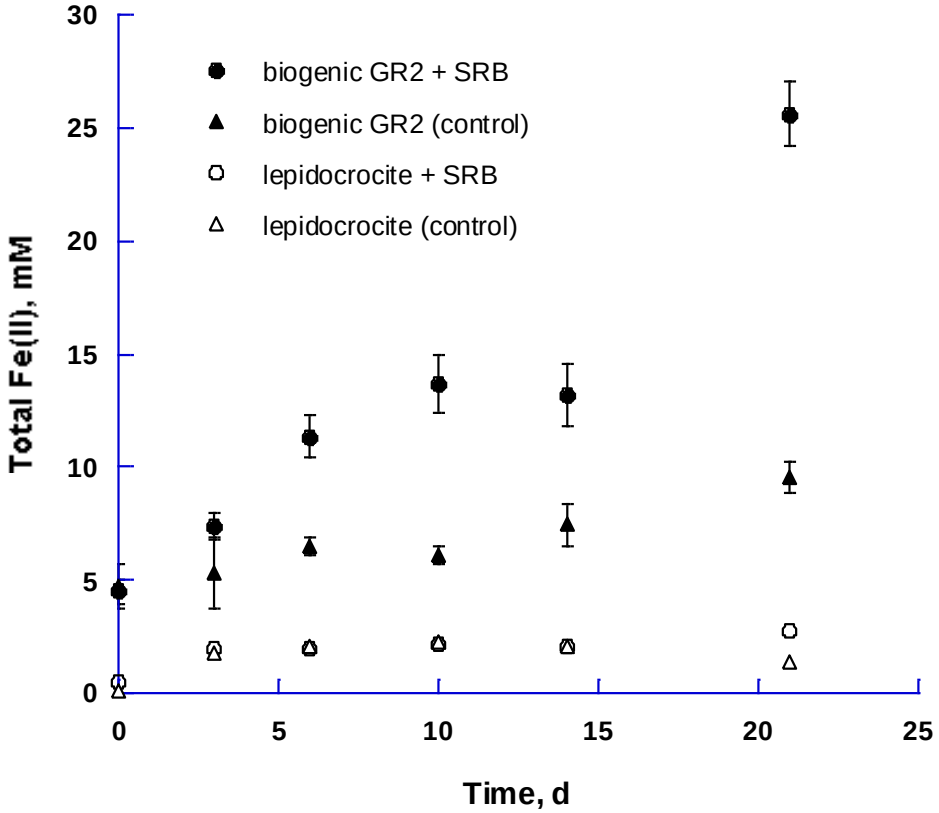
30
25
20
15
10
5
0
0
5
10
15
20
25
Total Fe(II), mM
Time, d
biogenic GR2 + SRB
biogenic GR2 (control)
lepidocrocite + SRB
lepidocrocite (control)

Figure 1

A)

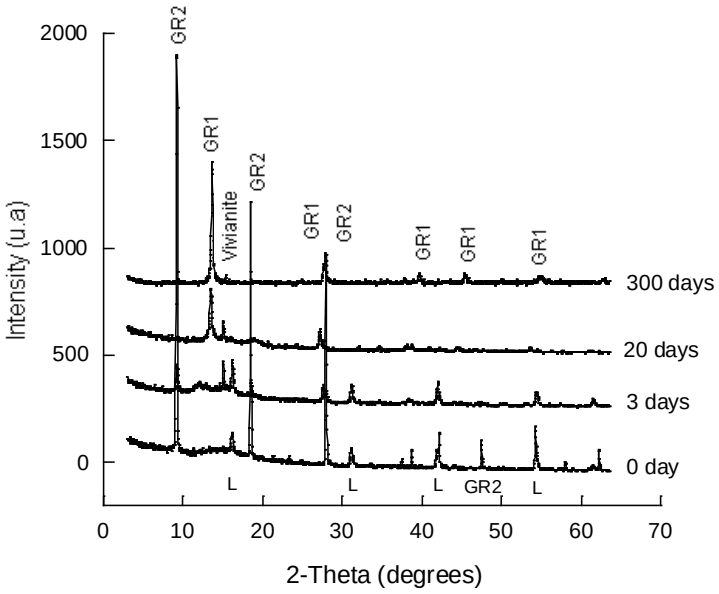
GR2
GR1
GR2
Vivianite
GR1
GR2
GR1
GR1
GR1
300 days
20 days
3 days
0 day
L
L
L
GR2
L
Intensity (u.a)
2-Theta (degrees)

B)

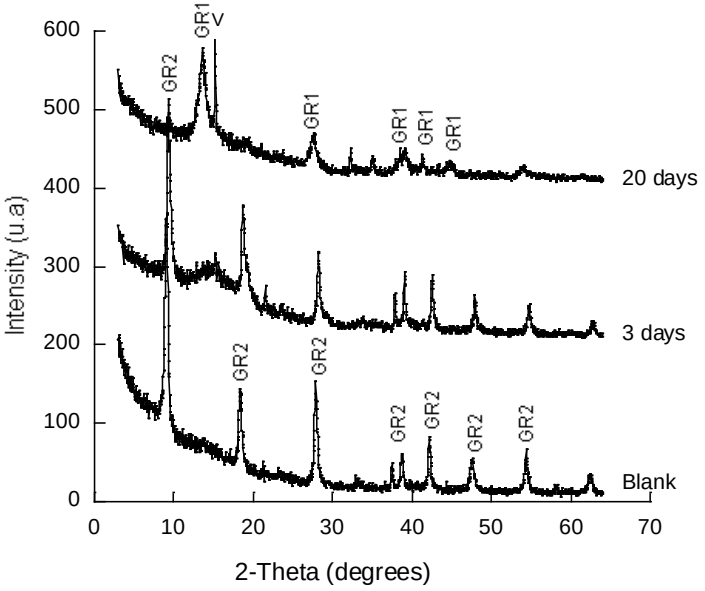
GR1
V
GR2
GR1
GR1
GR1
GR1
20 days
3 days
GR2
GR2
GR2
GR2
GR2
GR2
Blank
Intensity (u.a)
2-Theta (degrees)

Figure 2

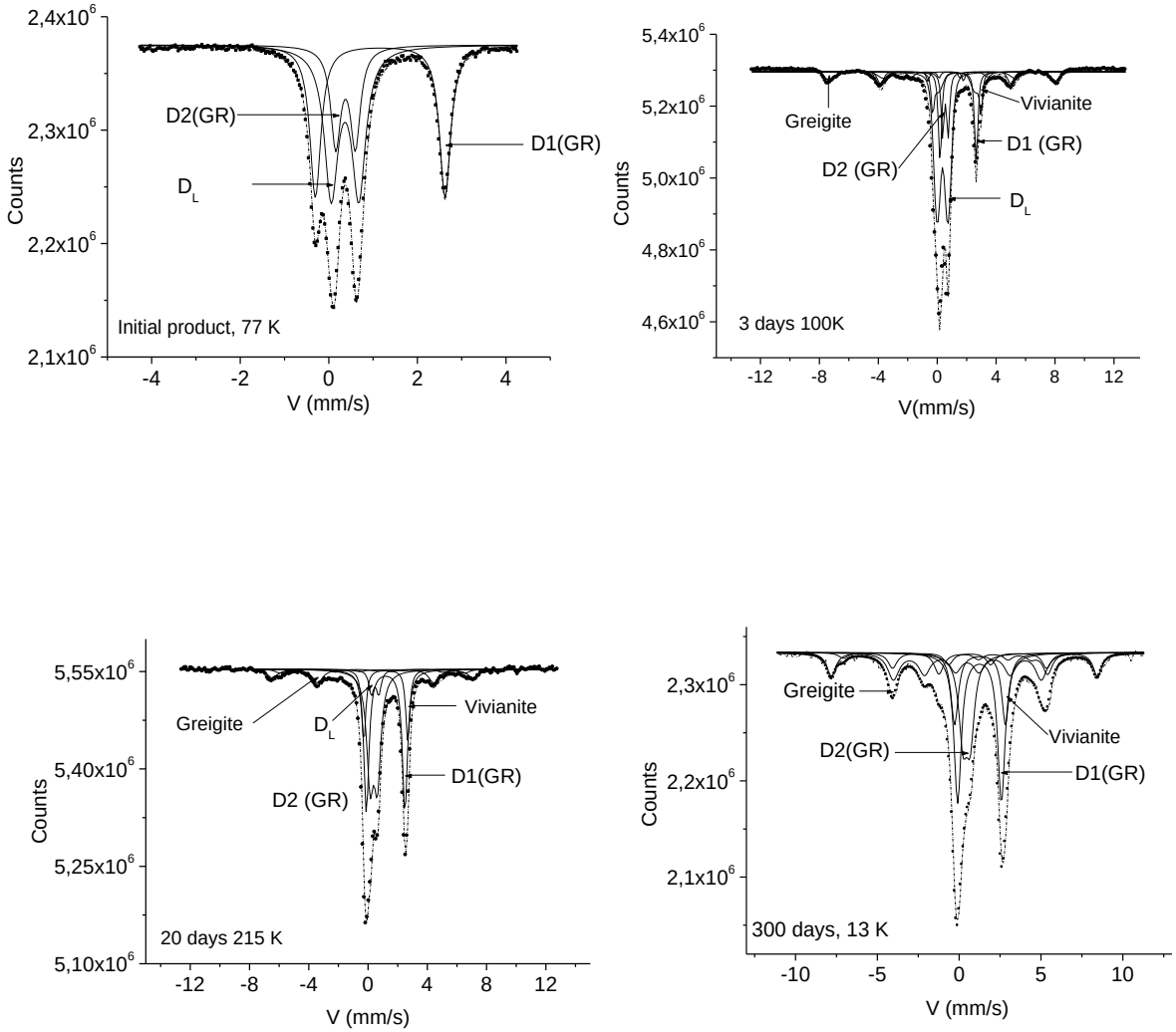
Counts
V (mm/s)
Initial product, 77 K
D2(GR)
D1(GR)
D_L
3 days 100K
Greigite
Vivianite
D1 (GR)
D2 (GR)
V(mm/s)
20 days 215 K
300 days, 13 K

Figure 3

A)

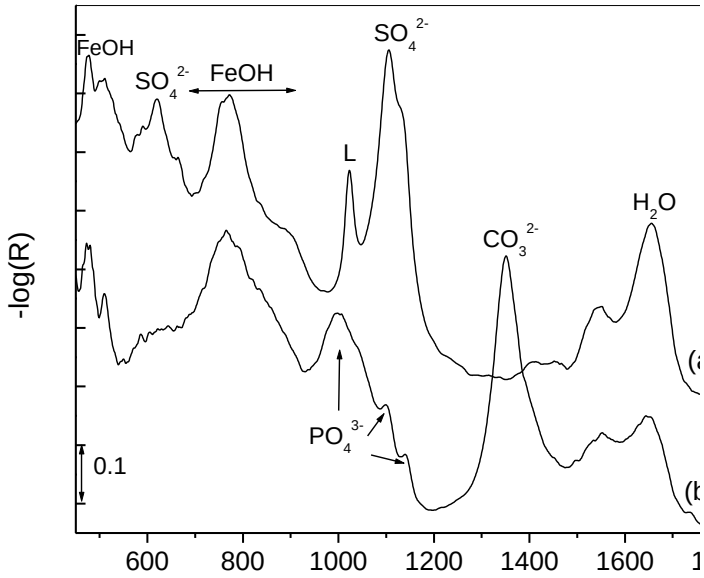
FeOH
SO4 2-
FeOH
SO4 2-
L
H2O
CO3 2-
PO4 3-
0.1
-log(R)
600
800
1000
1200
1400
1600

B)

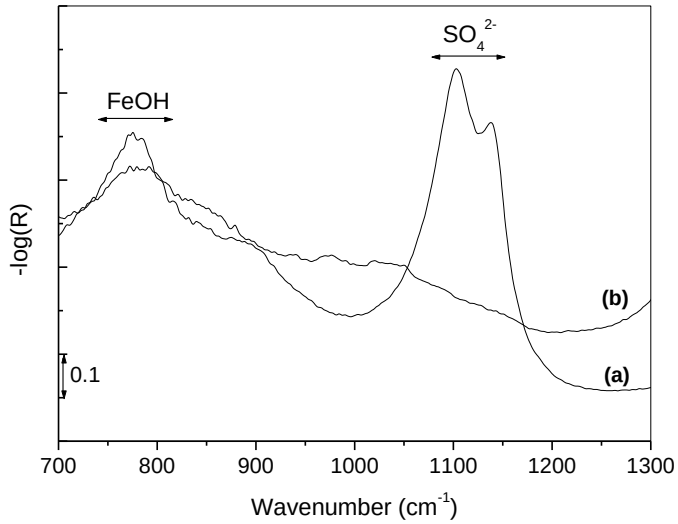
SO4 2-
FeOH
(b)
(a)
0.1
-log(R)
700
800
900
1000
1100
1200
1300
Wavenumber (cm-1)

Figure 4

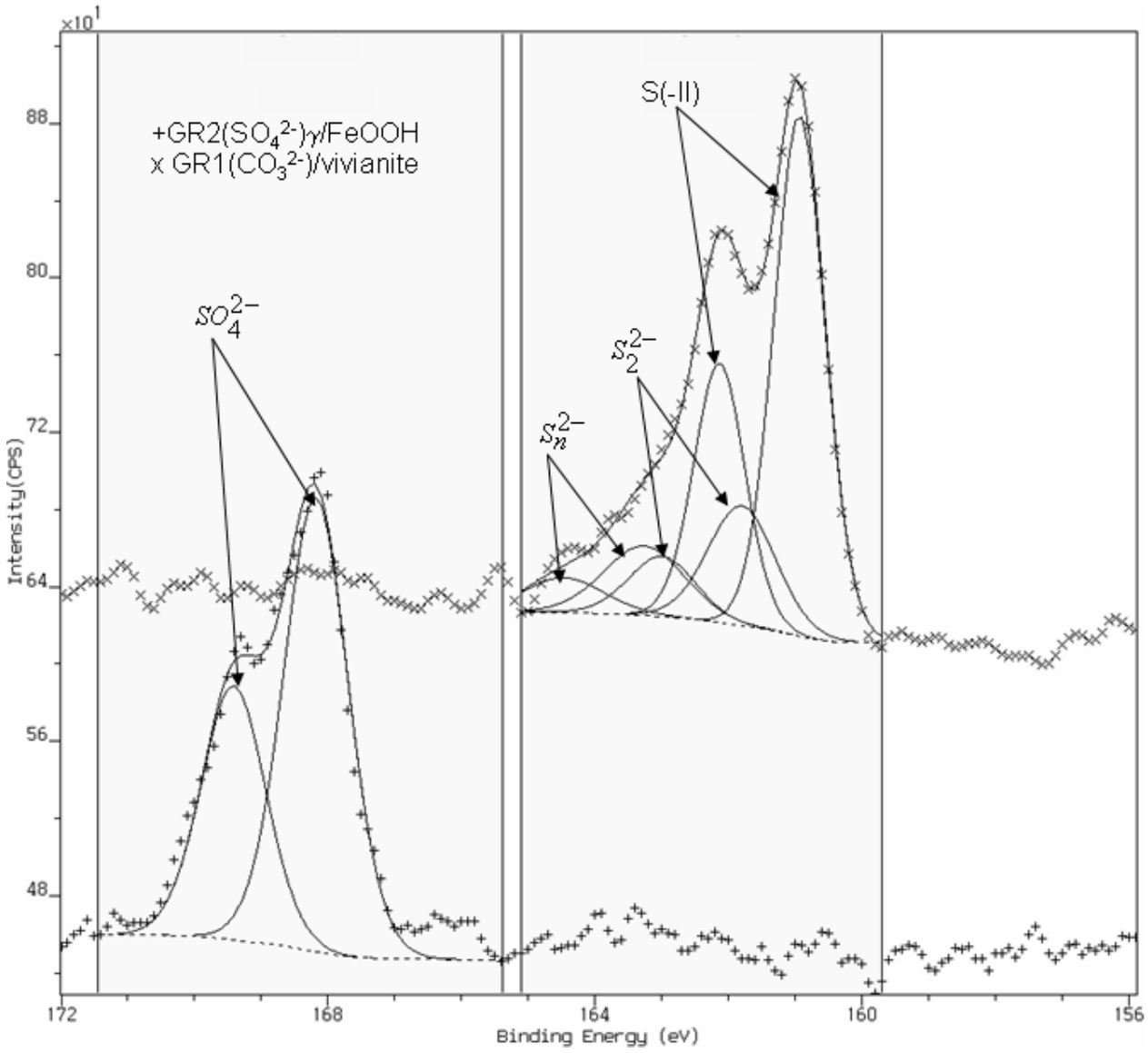
x10^1
88
80
72
64
56
48
Intensity(CPS)
+GR2(SO4 2-)γ/FeOOH
x GR1(CO3 2-)/vivianite
S(-II)
SO4 2−
S2 2−
Sn 2−
172
168
164
160
156
Binding Energy (eV)

Figure 5

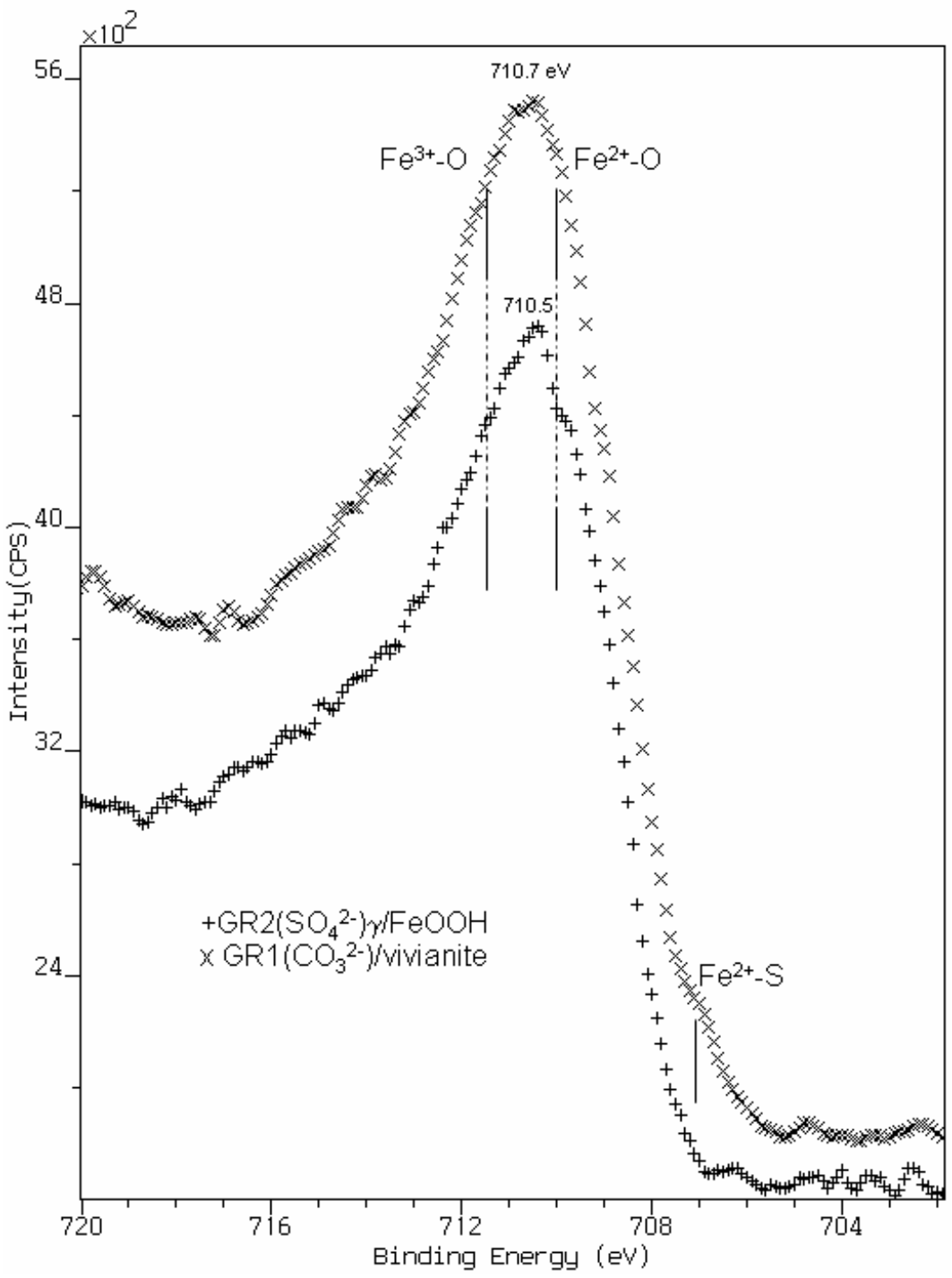
×10²
56
48
40
32
24
Intensity(CPS)
710.7 eV
Fe³⁺-O
Fe²⁺-O
710.5
+GR2(SO₄²⁻)γ/FeOOH
x GR1(CO₃²⁻)/vivianite
Fe²⁺-S
720
716
712
708
704
Binding Energy (eV)

Figure 6

A)

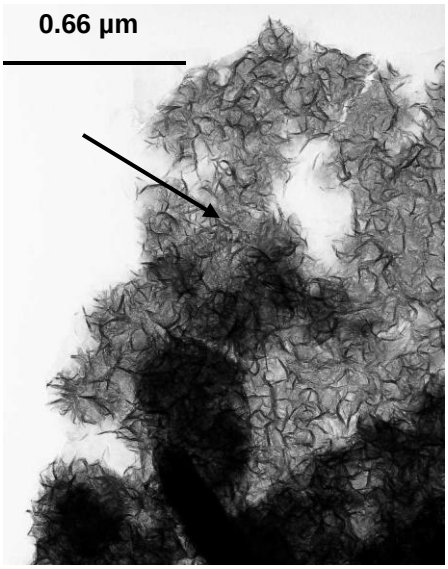
0.66 µm

B)

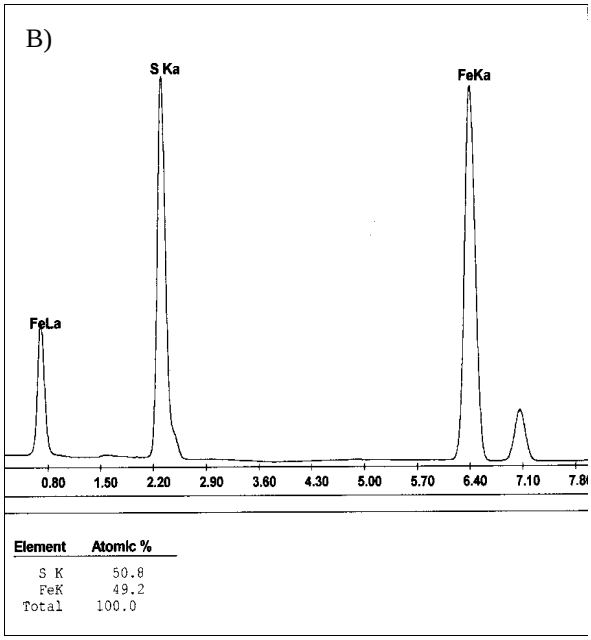
S Ka
FeKa
FeLa
0.80
1.50
2.20
2.90
3.60
4.30
5.00
5.70
6.40
7.10
Element Atomic %
S K 50.8
FeK 49.2
Total 100.0

Figure 7

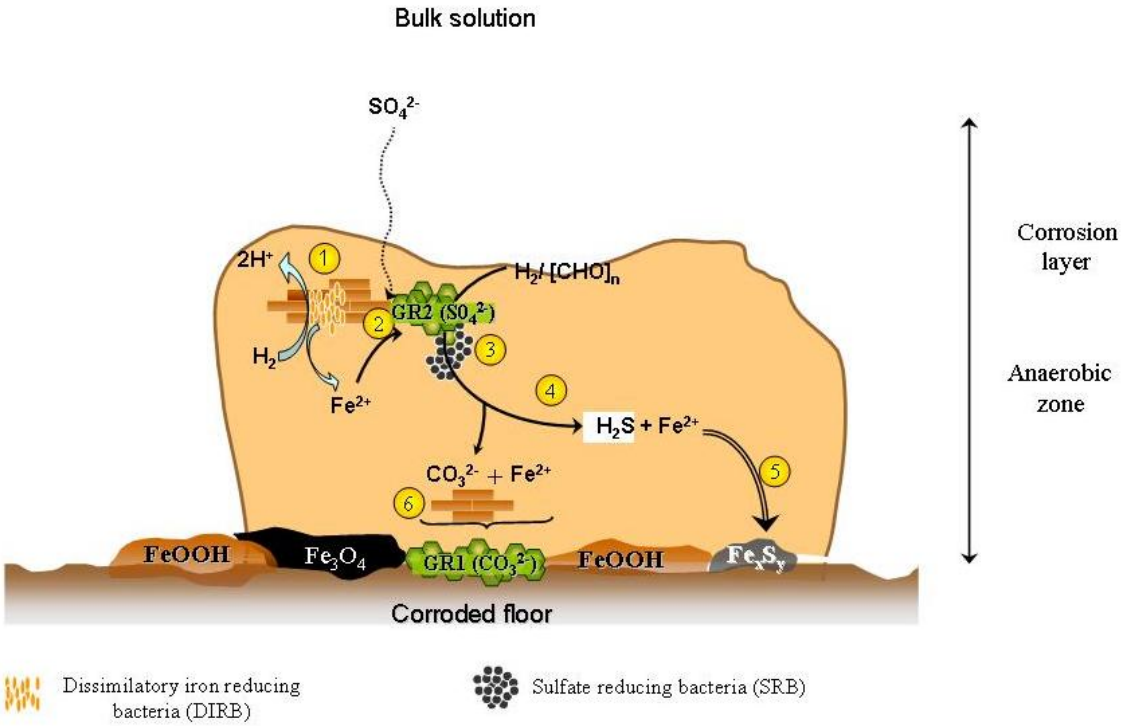
Bulk solution
SO_4^{2-}
$2H^+$
1
H_2/[CHO]$_n$
GR2 (SO_4^{2-})
2
3
H_2
Fe^{2+}
4
$H_2S + Fe^{2+}$
5
$CO_3^{2-} + Fe^{2+}$
6
FeOOH
Fe_3O_4
GR1 (CO_3^{2-})
FeOOH
Fe_xS_y
Corroded floor
Corrosion layer
Anaerobic zone
Dissimilatory iron reducing bacteria (DIRB)
Sulfate reducing bacteria (SRB)

Figure 8

Figure captions

Figure 1 Monitoring of the total ferrous ion (in the solid and aqueous phase) production during the incubation of the mixture of GR2(SO_4^{2-}) and lepidocrocite with *D. alaskensis* during the 21 days of incubation. Error bars show ± standard deviation of n = 4 cultures.

Figure 2 XRD spectra of the mineral solids from the treatments with *D. alaskensis* on biotic GR2(SO_4^{2-}) plus lepidocrocite (Fig. 2A) and abiotic GR2(SO_4^{2-}) (Fig. 2B) after different incubation time (day 0, day 3, day 20 and day 300). Green rust 2, lepidocrocite, green rust 1 and vivianite peaks are indicated by GR2, L, GR1, V respectively.

Figure 3 TMS spectra of solid phase obtained at different times of incubation (day 0, day 3, day 20 and day 300).

Figure 4 Infrared spectra of the mineral solid from the from the treatments with *D. alaskensis* on biotic GR2(SO_4^{2-}) plus lepidocrocite and abiotic GR2(SO_4^{2-}). Fig. 4A gives spectra for (a) GR2(SO_4^{2-})/γ-FeOOH minerals and (b) 300 days after SRB inoculation. Fig. 4B displays spectrum of (a) abiotic GR2(SO_4^{2-}) and (b) 20 days after SRB inoculation focused on the spectral range of sulfate adsorption (1300-700 cm^{-1}). (L: lepidocrocite). Before analysis each mineral was kept in an anaerobic chamber for 24 h under 90% relative humidity.

Figure 5 XPS Fe($2p_{3/2}$) spectra of (a) GR2(SO_4^{2-})/γ-FeOOH minerals and (b) 300 days after SRB inoculation.

Figure 6 XPS S(2p) spectra of (a) GR2(SO_4^{2-})/γ-FeOOH minerals and (b) 300 days after SRB inoculation. The vertical lines (from left to right) indicate the biding energies of Fe^{3+}-O, Fe^{2+}-O and Fe^{2+}-S respectively.

Figure 7 (A) TEM image of solids formed after 20 days of incubation. The arrow indicates FeS compound, whose composition is determinate by the SAED analysis (B).

Figure 8 A model of DIRB and SRB interaction via GR2(SO_4^{2-}) formation during a corrosion process of an iron surface in sea water. Representative SRB cells inside a tubercle of corrosion are shown. The hypothetical reactions occurring during DIRB and SRB interactions are numbered (path 1→6) and are issued from the following references. Reaction n°1, (Zegeye et al., 2005, reaction n°2, (Géhin et al., 2002), reaction n°3, 4, 5, (this study) and reaction n°6, (Drissi et al., 1995). Details are provided in the text.

Table captions

Table 1 Mössbauer parameters of solid phase obtained at different times of incubation (day 0, day 3, day 20 and day 300).

Table 2 Binding energies for S($2p_{3/2}$) and Fe($2p_{3/2}$) peaks in various model compounds.

Table 3 XPS peak fit parameters: peak energy, FWHM and area ratio of the S(2p) spectra. Binding energy peak location is accurate to 0.1 eV. Area for S(2p) includes $2p_{1/2}$ and $2p_{3/2}$ contributions.